Indian J. Phys. **67A** (2), 133-162 (1993)

The piercing view of an atom through energetic collision experiments : a case of multiple ionization

R Shanker and M J Singh
Atomic Physics Laboratory, Department of Physics, Banaras Hindu University, Varanasi-221 005, India

Received 16 July 1991, accepted 29 October 1992

Abstract : The objective of this review article is primarily to give an overview of the production of the energetic heavy ions by various particle accelerators in the country and around the world and further to use them for atomic physics experiments. An effort has been made to bring out an exposition of the heavy-ion 15 UD pelletron machine which has been recently installed as a "National Facility" for the University users at the Nuclear Science Centre (NSC), New Delhi. Possible major research areas aiming to utilize the facility are mentioned. The relevant theoretical models to interpret the processes involved in multiionization of atoms or ions are also summarized. A few experimental techniques to study the primary and multiionization processes are illustrated. In addition, some effort has been devoted to give a brief description of the parallel plate avalanche counter (PPAC) and the micro channel plates (MCP) detectors which are very often employed in accelerator based atomic physics experiments.

Keywords : Pelletron accelerators, multiple ionization processes, recoil ions, time-of-flight, spectrometer, microchannel plates.

PACS Nos. : 34.50.Fa, 29.17.+w, 29.20.– c

Plan of the Article

1. Introduction

The basic objective of the present article is to bring out scope, potentiality and application of an accelerator based atomic-physics, which when employed can furnish a deeper insight into the atomic structure and a detailed knowledge of the quantum electrodynamic processes involved in heavy-ion-atom collisions. In particular, the atomic-physics experiments which are being performed elsewhere or being planned with the heavy-ion pelletron facility at the Nuclear Science Centre (NSC), New Delhi, will be considered and discussed. The primary goal and the background of the article are directed to deal with an experiment on "The production and studies of the highly charged slow-moving recoil ions in heavy-ion bombardment with neutral atoms".

Before we dwell upon the actual topic, let us discuss what the NSC and its objectives are ? The NSC is located in the JNU (New) Campus, New Delhi, and is an autonomous Institution under the University Grants Commission (UGC). The major efforts of the centre are directed to create a culture of experimental sciences, to bring in creativity and collaborative atmosphere in high technology development in the Universities, in not only nuclear sciences but in all sciences like, chemistry, biology and in many applied areas such as, agriculture and medical sciences. Presently, the main research programmes being carried out in the NSC facility include experiments in nuclear physics, atomic physics, material science and radiation biology.

A detailed information about the structure of an atom can be obtained through well known techniques, for instance, the photoelectron spectroscopy, laser induced flouroscence (LIF) and the conventional spectroscopic methods. However, other equally important aspect of the atoms, namely, their collisional dynamics, excitation/ionisation mechanisms, charge transfer processes etc. which are found to play a key role in interpreting the data for plasma physics, astrophysics, atmospheric physics and in quantum electrodynamics, can be best understood by performing the accelerator–based atomic-physics experiments with a greater reliability and utmost precision [1].

The article is divided into seven sections : In the first section, the scope of accelerator based atomic physics has been outlined whereas Section 2 deals with various accelerators in the country and around the world. The theoretical background for understanding the multi-ionisation processes in heavy-ion atom collisions has been discussed in Section 3. Section 4 summarises certain aspects of the experimental techniques employed in understanding the primary ionisation processes. Various reaction channels in heavy ion-atom collisions have been discussed in Section 5. In Section 6, the two radiation detectors, namely, parallel plate avalanche counter (PPAC) and microchannel plates (MCP) have been described in some detail with regard to their working principles, characteristics and energy/time resolutions. Finally, Section 7 gives the summary of the main points in the article.

2. Charged particle accelerators

With the knowledge of an atomic nucleus and of its surrounding electrons, it was soon realised that the ions (i.e the atoms with one or more missing electrons from their ground state configuration) can be produced with great efficiency and they can be further accelerated by applying high voltages. These energetic ions can be employed to probe the atoms and the nuclei to study their structures because the probe ion's de-Broglie wavelength can be made extremely small. Such a d.c. high voltage machine is commonly called an "accelerator". These machines have been developed and used at various places in the last six decades around the world. Some of these machines are listed in Tables 1 and 2.

Table 1. A few particle accelerators around the world, built and operated initially.

Date	Accelerator	Energy/particle
1932	Cockcroft–Walton (Cavendish Lab., U.K.)	Upto 0.5 MeV protons
1957	Proton synchrotron (Synchrophasotron) Dubna, U.S.S.R.	Upto 10 GeV protons
1959	CERN alternating–gradient proton synchrotron, Switzerland	Upto 28 GeV protons
1966	Stanford 2–mile linear accelerator (SLAC). Stanford University, U.S.A.	Upto 20 GeV electrons

Table 1. (*contd.*)

Date	Accelerator	Energy/particle
1967	Alternating gradient proton synchrotron, Serpukhov U.S.S.R.	Upto 76 GeV protons
1977	National accelerator lab. proton synchrotron, Weston I11., U.S.A.	Upto 500 GeV protons
1980	Pelletron machines (heavy-ion) N.E.C., U.S.A.	Several MeV/nucleon

Source : Ref. : [2]

Table 2. Accelerators around the country

1) Saha Institute of Nuclear Physics, Calcutta
   - i) 4 MV, 38 inch cyclotron
     Proton Beam : Internal 50-70 μA at 4 MeV
     External 0.1 μA at 4 MeV
   - ii) 400 KV : Cockroft Walton accelerator

2) Tata Institute of Fundamental Research (TIFR), Bombay
   - i) 300 kV : Oper air Van de Graaff accelerator
   - ii) 1 MV : Electron linear accelerator
   - iii) 1 MV : Cockcroft-Walton accelerator
   - iv) 14 UD : Pelletron heavy ion machine

3) B. H. U., Varanasi
   400 kV : Van de Graaff accelerator

4) A M. U., Aligarh
   150 kV : Neutron generator

5) BARC, Trombay, Bombay
   - i) 5.5 MV : Van de Graaff accelerator
   - ii) 2 MV : Tandem accelerator

6) I.I.T., Kanpur
   2 MV : Van de Graaff accelerator

7) I. I. Sc., Bangalore
   2 MV: Electron Van de Graaff

8) Variable Energy Cyclotron (VEC), Calcutta

9) 3 UD : Pelletron at Institute of Physics, Bhubhaneshwar

10) 8 MV : Microtron accelerator, Pune

11) Electron storage ring (Synchrotron radiation source), CAT, Indore (commissioned).

Recently, a heavy ion machine called the 15 UD Pelletron Tandem accelerator capable of furnishing proton energy upto 32 MeV has been installed by the Electrostatic International Inc., Madison, WI, U.S.A., at the Nuclear Science Centre, New Delhi, as a National facility especially meant for the University users under the financial assistance from U.G.C., New Delhi. A detailed information about the machine is given in the following paragraphs.

2.1. The 15 UD pelletron accelerator :

The 15 UD pelletron machine is built in a tandem configuration and is essentially a Van de Graaff accelerator in which the charge carrier belt is replaced by a chain of pellets. The number 15 stands for 15 Million Volts terminal voltage* and UD stands for Unit Double. The whole machine is mounted vertically so that it saves much of the space it would occupy in the horizontal mounting.

The basic components of the machine can be listed as follows :

a) Negative ion source,
b) Injector magnet,
c) Accelerator columns and the terminal,
d) Strippers,
e) Analysing magnet, and
f) Switching magnet and beam transportation system.

2.2 Working-principle and the machine's configurations :

The negative ions are usually produced in three types of ion-sources, viz. (i) the direct extraction duoplasmatron source, (ii) the Cs-enhanced negative ion sputter source and (iii) the negative-helium ion source. They are located in a source room sitting at top of the machine. The negative ions of almost all elements of the periodic table except inert gaseous ions (excluding He ions) are injected into the main accelerating column at 90° via an injector-magnet and a quadrupole lens at energies between –50 and –380 keV. The terminal voltage platform situated in the middle of the machine can be varied from +4 MV to +16 MV using an electrostatic charge transfer device. The negative ions are extracted on to the terminal and stripped out to their positive charge states by using either a column of gaseous strippers or thin foils. Normally, nitrogen and carbon are used as gaseous and solid strippers respectively. Finally, these positive ions are once again brought down to earth potential by gaining a further 16 MV accelerated energy. Thus , heavy-ion of charge state z will obtain its final kinetic energy equal to $(z + 1) \times 16$ MeV. The proton when accelerated to a full terminal voltage will gain energy of 32 MeV. The accelerating columns are evacuated upto a pressure better than 10^{-8} Torr by using high efficiency turbo molecular– and cryo-pumps. The accelerating cascades are immersed in a large tank filled with an insulating gas (SF_6) at a high pressure (10 kg/cm^2) to prevent sparking/discharges etc. The emerging positive ions are then finally analysed by a powerful magnet with respect to their energies and charge states and are bent at 90° with respect to the vertical position for transporting them to the beam hall through a switching magnet. The full sketch of the machine is shown in Figure 1 with essential dimensions marked therein. In normal mode of operations, one can get a d.c. beam; however, provisions are there to obtain a pulsed beam by employing a dual bunching/pulsing unit just after the injector quadrupole units (not shown). The beam

* The usable terminal voltage has been increased from 15 MV to 16 MV by using the compressed geometry accelerator tubes.

transport and focussing systems are interfaced with a computer and have been supplied by Danfysik, Denmark. The accelerator is controlled and monitored by a PDP 11/73 computer. The typical parameters of the 15 UD pelletron machine are given in Table 3.

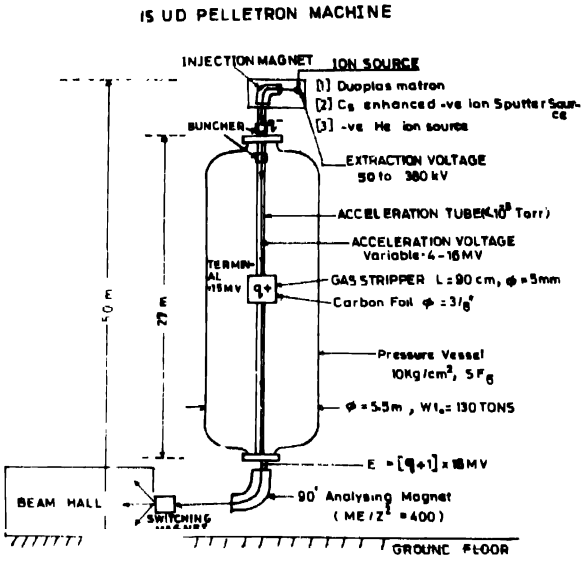

Figure 1. Schematic diagram of the 15 UD pelletron machine installed at NSC, New Delhi.

Table 3. Typical parameters of the 15 UD pelletron machine at NSC.

Ion sources : i) Direct extraction duoplasmatron source	
ii) Cs enhanced negative ion sputter source	
iii) Negative helium ion source	
Terminal voltage	4 – 15 MV
Mass number of ion	1 – 240
Ion injection energy	50 –380 keV
Injector magnet	$ME/Z^2 = 80$
Diameter of the pressure vessel	5.49 m
Length of the pressure vessel	26.57 m
Diameter of the column	1.32 m
Length of column (including terminal)	22 81 m
Diameter of the terminal	1.52 m
Length of the terminal	3.81 m
Strippers : i) Gas stripper (N)	Length = 0.90 m
	Diameter = 5.0 mm
ii) Foil stripper (Carbon)	Thickness = 3/8"
Charging system	Double pelletron chain
Beam current (d c)	Proton – 5 0 μA at 30 MeV
	Alpha – 2 0 μA at 45 MeV
	Nickel – 0 2 pμA at 15 MV terminal voltage
Beam current (pulsed)	Proton – 0 5 mA at 28 MeV
(Pulsed peak value)	Nickel – 4 0 pμA at 15 MV terminal voltage
	Iodine – 4 0 pμA at 15 MV terminal voltage
Pulse width	< 3 ns
Pulse repetition time	4 μ sec. in steps of 250 ns
Analysing and switching magnets	Analysing magnet . $ME/Z^2 = 400$
	Switching magnet : $ME/Z^2 = 295$ at 30° (with seven ports)

Source : Ref. [3]

3. Multi-ionisation processes in heavy ion-atom collisions

When a fast moving (MeV/amu) ion collides violently with a multielectron atom, some translational energy of the projectile is deposited into the electronic degrees of freedom of both collision partners [4]. In this process, those electrons which have their binding energies close or less than $\frac{1}{2}m_e v_p^2$, are ionised and excited with appreciable probabilities :

where, m_e and v_p refer to the mass of the electron and the velocity of the projectile respectively. Consequently, the target and the projectile emerge from the collision region in highly ionised and excited states.

It should be noted that the ionisation process is a velocity dependent one and the translational energy of the projectile is larger than the electronic excitation or the ionisation energy $1/2\ m_e v_p^2$, by a factor M_T/m_e. This ratio is typically several thousand. In the collision, the target atom, however, acquires a translational energy much less than the energy deposited for its electronic excitation or ionisation. This is so because the nuclear stopping power is several orders of magnitude smaller than the electronic stopping power for the fast ions. Thus, we may say that the target atom, after collision is Electronically HOT but Translationally COLD.

In order to understand this, let us consider a fast heavy ion collision system as shown in Figure 2.

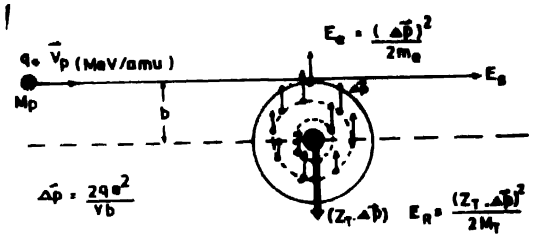

Figure 2. Vector diagram showing momentum balance between the initial projectile momentum and the final momenta of the projectile (p), the electrons (e) and the recoil (r).

If Δp is the transverse momentum transfer per unit charge by the projectile ion to the target atom in a straight line trajectory motion, then

the total transverse momentum transferred to the nucleus of the target atom = $z_T.\ \Delta p$

where, z_T is the atomic number of the target atom.

Consequently, the target atom gets this momentum and recoils with a translational energy (recoil energy)

$$E_R = \frac{(z_T.\Delta^2)p}{2M} \tag{1}$$

where M_T = Mass of the projectile atom/ion.

However, an electron of the target atom under consideration also gets the same transverse momentum Δp in the opposite direction to that of the nucleus (as electron being negatively charged particle). The corresponding electronic energy of excitation or ionisation is

$$E_e = \frac{(\Delta p)^2}{2m_e} \tag{2}$$

Hence, $$\frac{E_R}{E_e} = \frac{z_T^2 m_e}{M_T} \tag{3}$$

since the ratio (m_e/M) is very small $(<<10^{-3})$, $E_R << E_e$, this condition obviously leaves the target atom electronically HOT but translationally COLD.

In a straight–line collision, the impulse given to the recoil ion is finite only in the direction transverse to the projectile direction. The recoil energy can be calculated by using an expression

$$E_R \text{ (eV)} = \frac{1.8 \times 10.^{-20} r^2 . p^2}{M_T . E_p . \sigma_r} \tag{4}$$

where σ_r (in cm^2) is the observable cross section for producing recoil ions in the final charge state r by the projectiles in their final charge state $p.E_p$ is the energy in MeV per unit mass for the projectile.

For example, 1.4 MeV/amu U^{32+} + Ne collision system for which $\sigma_r = 3 \times 10^{-16}$ cm^2 (observed)

$r = 4+, p = 32+$

$E_R = 0.04$ eV.

using eq. (3), we obtain

$E_e = 15.0$ eV, which suggests that $\frac{E_e}{E_R} = 400$.

Furthermore, from eq. (4), it is seen that E_R increases as the final charge state of the recoil ions increases (due to r^2 dependence) and also due to $1/\sigma_r$ dependence (decreases rapidly with r). For the collision considered above, it is assumed that the potential (Coulomb) experienced by the projectile ions is much smaller than their kinetic energies.

3.1. Some attractive features of the slow-moving recoil ions :

(i) The slow (cold) moving highly charged (hot) recoil ions provide almost Doppler-free spectroscopy, *i.e.*, the Doppler broadening of the lines arising from recoil ions is negligible. This situation enables one to make high precision wavelength measurements.

(ii) The recoil ions offer the possibility to study collisions between highly charged ions of low velocities and target atoms as a SIRS (Secondary Ion Recoil Source).

(iii) The basic question on very low energy capture and transfer ionisation processes can be answered using SIRS experiments.

(iv) The recoil ion sources provide opportunity to do the laser-ion beam experiments for new and very precise information on atomic and nuclear structures.

(v) The data obtained using the SIRS experiments are expected to be useful in interpreting the processes which are very frequently involved in Astrophysics, Atmospheric physics and Plasma physics problems.

3.2. Theoretical approach :

Without going into the details of the theoretical modeling we shall describe briefly the theoretical approach which is commonly used for interpreting the data on multi-ionisation processes. This could be classified as given below :

3.2.1. Independent particle model (IPM) :

The basic features (assumptions) of the IPM [5] are :

(i) The electronic wave functions for the target atom can be represented by a product of the wave functions of the individual electrons. Thus the electron correlation is ignored and some type of effective potential is assumed for the motion of the electrons. Hence the effective potential may be a simple Coulomb potential with the screening parameters determined from Hartree Fock calculations or from a Thomas–Fermi potential.

(ii) The motion of the projectile is treated as a "classical" trajectory for which

$$\frac{2z_p z_T e^2}{\hbar v_p} >> 1 \tag{5}$$

is valid. v_p and v_e are the velocities of the projectile and that of the target electron under consideration respectively. z_p and z_T are the atomic numbers of the projectile and the target atoms respectively.

(iii) Ionisation probabilities for n-electrons of a shell of N–electrons of the target atoms are given by

$$P_n = \begin{bmatrix} N \\ n \end{bmatrix} . p_i^n \ (1 - P_i)^{N-n} \tag{6}$$

where, $\begin{bmatrix} N \\ n \end{bmatrix}$ are the binomial coefficients and P_i are the single electron ionisation/capture probability for the i-th electron.

However, this model is not reliable for high degree of ionisations, that is, for multiple ionisations : because the effective potential changes rapidly with multiple ionisation. A partial remedy to this problem is to employ a time-dependent effective charge for the target atom. Nevertheless, the IPM model is very attractive for the low stages of ionisation processes.

3.2.2. Statistical or energy deposition model :

In this model [6], the collision is assumed to proceed in two steps :

(i) The projectile and target collide, the transfer of kinetic energy of the projectile to the target atoms takes place.

(ii) The transfered K.E. is deposited into the electronic excitation or ionisation of the target atom and is distributed among its electrons leading to the final ionisation state. However, this model is unable to take account of the charge transfer processes which are known to be important collision mechanisms in the production of highly charged recoil ions.

The energy transfer from the projectile to the target atom is treated in a classical impulse approximation as a function of the impact parameter. The total energy deposited is calculated by integrating over the spatial probability distribution of each electron and finally, summing over the number of electrons of the target atom. The probability for each final ionisation is proportional to the volume of the phase space available to it and is directly related to the energy deposited in the collision and the ionisation energies of the various levels. This model, however, is found to underestimate the cross sections for low stages of ionisation.

3.2.3. Classical trajectory Monte-Carlo method :

The three- and *n*-body Classical Trajectory Monte–Carlo (CTMC) methods [7] have proved to be successful approximations to deal with the electron capture and ionisation processes in ion-atom collisions at energies sufficiently high, so that the molecular effects are not important.

In three-body CTMC calculations, the interacting particles : projectile ion, target and an active electron, 18- coupled first-order differential equations are solved corresponding to their x, y, z cartesian coordinates and their conjugate momenta. However, in *n*-body CTMC method, one has to solve $6(N+2)$ coupled first-order differential equations arising from the equations of motion, where, N refers to the total number of electrons of the target atom. In these calculations the electron–electron interactions are not included explicitly as a part of the Hamiltonian.

CTMC superiority over other methods :

(i) The electron – projectile ion and the electron target nucleus interactions are explicitly taken into account during the collision.

(ii) An accurate description of the quantum mechanical electron – momentum distribution is fully accounted for in the CTMC methods.

(iii) The CTMC model calculations provide for the first time a method to determine the recoil energies of the target ion and the angular scattering and energy loss of the projectile.

4. Experimental techniques

In this Section, we summarise certain techniques which are used to measure the characteristics of the primary ionization processes in ion-atom collisions. The description of

the technical setup appropriate to our present experiment is reserved for the latter part of this Section.

4.1. Total charge measurements :

Early experiments were performed to measure the total charge production by a passage of fast moving ion through a thin gaseous target. An electrical field orthogonal to the primary beam direction collects the recoil ions on a set of condenser plates parallel to the beam. The total charge collected (Q) for the outgoing projectile ions (N_s) is related to the total charge production cross section by

$$\sigma_+ (\text{cm}^2) = \sum_r r\sigma_r = \frac{1.87 \times 10^5 \, Q \, (\text{Coul.})}{N_s . \, l . \, p} \tag{7}$$

where, r = recoil ion charge state,

p = pressure of the target gas (in mTorr),

l = length of the interaction zone (in cm),

σ_r = total cross section for the production of recoils with charge state r.

Since only a charge weighted sum of the σ_+ are measured, such data provide only a gross test of the theoretical models.

4.2. Recoil ion mass spectroscopy :

The energetic beams of multiply charged ions are cross-fired with a thermal atomic beam at right angles. The recoil ions produced in an interaction zone are extracted by an electrostatic field into a retarding potential energy analyser (RPA) and are then focussed on to the entrance plane of a quadrupole mass spectrometer. The recoil ions analysed on the basis of

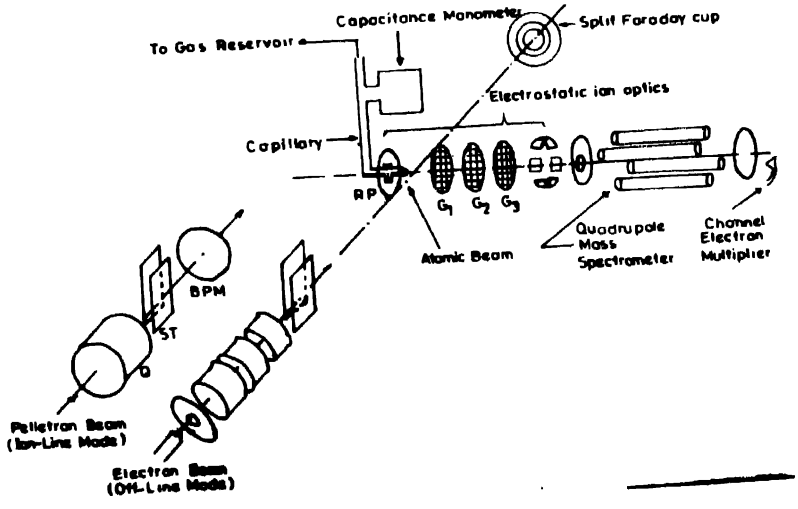

Figure 3. Typical set up for a recoil-ion mass spectroscopy (with the courtesy of D Mathur, Ref. 8).

their transverse kinetic energy and their mass to charge ratio are detected by an off-axis channel electron multiplier coupled to conventional pulse counting electronics and to multi-channel analyser. The fast-ion beam is collected downstream of the interaction zone by a position sensitive faraday cup. The recoil ions formed in the interaction zone are pushed into the RPA by a positive potential applied to a repeller plate (RP) placed over atomic source. A typical set up of the recoil ion mass spectroscopy [8] is shown in Figure 3. With such a kind of set up, one can determine the fraction of the recoil ions produced in the different charge states as a function of the charge states of the fast projectile beams. However, this method may not be suitable for determining the recoil ion production cross section differential in projectile scattering angle as here the mass spectra measured result from an integration over all the impact parameters and the charge states of all the projectile ions, thus giving the total cross section for the recoil ion production.

4.3. Time of flight (TOF) measurements :

Most recoil ion production cross section measurements have used an electric field orthogonal to the primary ion beam for extracting the recoil ions and have used the different flight times [9] of the ions to a distant detector to seperate the different charge states. If the primary beam is pulsed, the time zero is taken from the Master clock of the pulsing system. A d.c. beam can also be employed if one detects either the associated electrons or the scattered projectile ions of a selected charge state. Normally, sorting of the scattered ions are done by employing a magnetic analyser or an electrostatic deflector coupled with a position sensitive parallel plate avalenche detector (PPAD). The recoil detector is commonly a channeltron or a micro channel plate (MCP) which is capable of giving a sub-nanosecond timing. Overall time resolution of the system is more or less limited by geometrical considerations than by electronic timings.

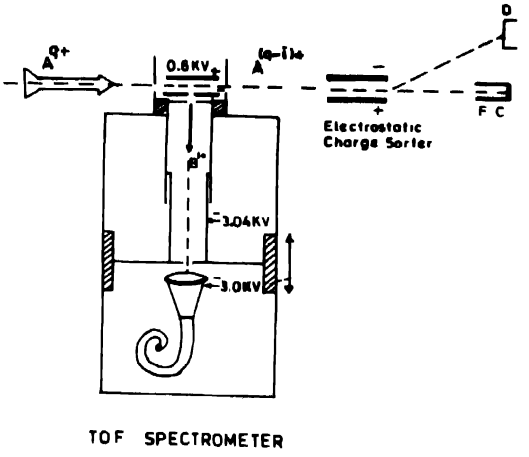

Figure 4. Schematic of the time-of-flight spectrometer.

A schematic time-of-flight spectrometer is shown in Figure 4. Refering to this figure, if ions of charge state r and mass M_T are created at rest ($E_R = 0$) in an electric field of strength ε, accelerate over a distance d_1 and subsequently drift freely an additional distance d_2 to the detector, the flight-time to the detector is given by

$$t\,(\mu\,\text{sec}) = 0.72\sqrt{\frac{M_T}{\varepsilon.r.d_1}}\,(2d_1 + d_2) \tag{8}$$

where, M_T is expressed in a.m.u., ε in volts/cm and distances in cm.

It can be readily shown that time-focusing can be achieved if $d_2 = 2d_1$. The time defocusing occurs due to the finite lateral spread in the primary ion beam. A major advantage of the TOF spectrometer is that, by virtue of its simplicity, the efficiency and the solid angle are quite independent of charge or mass of the recoil ions. Thus, a simple normalization is adequate for all cross sections if one of them has been normalised to a known cross section for the production of the singly charged recoil ions by light projectiles. In our present experimental set up, we are employing the TOF method to study the Ar recoil ions produced in interaction of 60 MeV $O^{5+,\,6+}$ ions with Argon gas atoms. The corresponding experimental set up for studying the recoil ions is shown in Figure 5, wherein the charge selection of the scattered projectile is to be performed by a system employing a combination of an electrostatic deflector and a position sensitive parallel plate avalanche detector (PPAD). This set up will enable us to study not only the differential cross sections but also the processes that distinguish the electron captures from those of direct ionization.

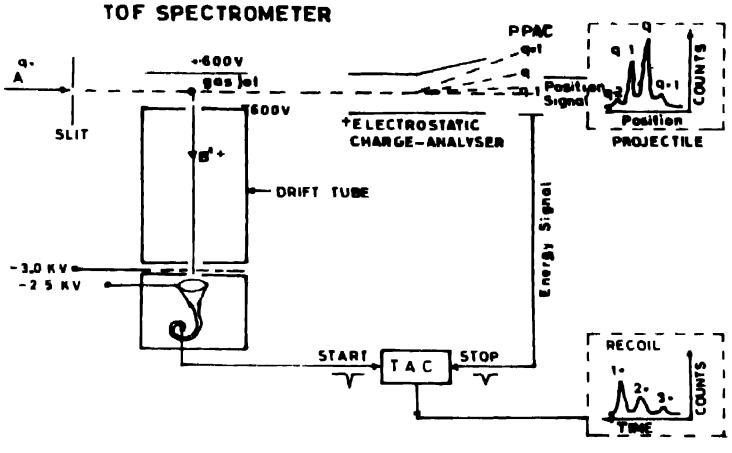

Figure 5. Experimental set up for studying recoil ions at NSC, New Delhi.

5. Fast ion-atom collisions and reaction channels

The production of various reaction channels in a violent collision between a fast-moving heavy-ion and a thermal atom can be understood by considering the following typical example :

$$A^{q+} + B = A^{q'+} + B^{i+} + (q' - q + i)\, e \qquad (9)$$
$$= A^{q'+} + B^{i+} + (k + i)\, e$$

where, $k = |q' - q|$ = charge transfer of the projectile.

Three cases arise :

(i) if $k > 0$, loss–ionization

(ii) if $k = 0$, direct ionization

(iii) if $k < 0$, electron–capture (transfer-ionization).

For case (i) the projectile ion loses its k-electrons in the collision via a direct-ionization process with simultaneous ejection of i electrons from the target atom. The case (ii) corresponds to the process in which the projectile undergoes no change in its charge state (k=0) but accompanies the recoil ions loosing their i-electrons through direct ionization process. For case (iii), the two processes are invloved in the same collision event; one of the target electrons is ionized and other is captured by the projectile ion. This process is commonly called the transfer-ionization (TI) process. All the above three cases are planned for studies under the present investigations.

If $\sigma^{i}_{q,q'}$ refer to the partial cross sections of Ar recoil ions in the considered collision system, then the projectile charge changing cross section $\sigma_{q,q'}$ summed over partial cross sections of Ar-recoil ions with different charge i are given by

$$\sigma_{q,q'} = \sum_{i} \sigma^{i}_{q,q'} \qquad (10)$$

where, q and q' are the projectile charges before and after the collision respectively.

Further, the average charge $\langle i \rangle_{q,q'}$ of Ar-recoil ions produced is given by

$$\langle i \rangle_{q,q'} = \sum_{i} \frac{i.\ \sigma^{i}_{q,q'}}{\sigma_{q,q'}} \qquad (11)$$

In an analogous way, if one records the projectile charge spectrum by counting the coincidence events corresponding to a fully opened window of the recoil ions and of the scattered projectiles, then the average charge change of the projectiles $\langle k \rangle$

$$\langle k \rangle = \sum k F_k \qquad (12)$$

where, F_k is the fraction of projectiles whose charge changes by k and can be determined by the projectile charge spectrum.

The measured time-of-flight spectrum of the Ar-recoil ion produced in 1.0 MeV/amu F^{q+} + Ne collisions are shown in Figure 6 (a–c) taken from reference [10] as typical examples. From these spectra, it is noted that the 2-electron capture by the projectiles

makes important contribution to the production of the higher recoil charge states (i = 6+, 7+, 8+). Similar data on other collision systems for the recoil ion production cross sections, direct-ionisation, electron-capture cross sections have been obtained by various workers [11-13]. It has been remarked that uptil now, very few experimental as well as theoretical investigations have been devoted towards studying the mechanism of recoil ion production when the loss ionisation of the projectiles with a number of screening electrons is accompanied simultaneously. However, [14] have developed a new TOF spectrometer for measuring the projectile dependent atomic excitation and ionisation cross sections at very small scattering angles of $< 10^{-4}$ rad. They have found that the measured transverse recoil energy is a well defined function of the scattering angle. In order to fully understand the multiple ionisation of target atoms, further accumulation of experimental data is required. Investigations of the related topics such as, the impact parameter dependence is also important to some extent. Recent efforts are in fact, directed in achieving these objectives.

6. Detectors

In Atomic collision experiments, one normally employs most of the detectors and the techniques that are used in Nuclear physics experiments. We, therefore, give a brief report on the selected nuclear radiation detectors : their working principles, characteristics and energy domains etc., particularly of those which are most suitable for detecting radiations and particles emitted from atomic (ionic) collisions with matter. In particular, two detectors, namely, the parallel plate avalanche counter (PPAC) and the microchannel plate (MCP) have been chosen and presented here in some detail.

The charged particles which include electrons, protons, alpha particles and other energetic atomic ions interact with matter primarily through Coulomb fields, resulting in ionization and excitation of atoms and molecules of the medium. These events of excitation and ionization are so numerous that the energy loss of the incident particles is very nearly continuous. The ionization events result into the creation of free charge carriers capable of drifting in an external electric field. The excitation and ionization of the medium atoms and molecules result into the emission of photons, ions and electrons. A majority of detectors rely on sensing either the free charge carriers or the photons. Based on this principle, the detectors for the charged particles can be broadly classified as :

(a) Ionization based detectors : These detectors sense the free charge carriers.

(b) Scintillation detectors : They sense the luminescence photons arising from the decay of excited species of interest.

(c) Track visualisation detectors : They make the ionization columns or tracks visible along the trajectory of impinging charged particles.

(d) Neutral radiation detectors : Neutral radiations cannot interact with matter either through ionization or scintillation processes. Their detection is made possible by a two step process : ((i) liberation of an energetic charged particle via some interaction of neutral radiation with matter, (ii) detection of the liberated charged particles.

Different types of detectors and the type of particles they can detect, are grouped together in Table 4.

Table 4. Types of Radiation Detectors, their principles and applications.

Detector	Principle	Detecting system	Particle detected	Applications
Ionisation chamber	Ionisation of gases	Air	Alpha	Measurement of activity
Ionisation chamber (with grid)	Ionisation of gases	Ar + CO_2	Alpha, fission fragments	Energy measurement if particle stops in chamber
Proportional counter	Ionisation of gases	Ar + CH_4	Alpha, beta electrons	Measurement of energy
G.M. Counter	Ionisation of gases	Ar + Cl_2	Alpha, beta gama, cosmic rays	Good for intensity determination
Parallel plate avalanche counter	Ionisation of gases	Hydrocarbons	Alpha, fission fragments	Timing and position information
Solid State detectors				
Few microns to a few mm in thickness	Electron-hole pair production	Si doped with Li, P or B	Alpha, beta proton fission products	Detection of charged particles. Measurement of energy
Few mm to 10 cm in thickness	Electron-hole pair production	Ge doped with Li	Gamma	Energy discrimination but low efficiency
Micro channel plate (MCP)	Electron multiplication	Semi-conducting lead	Electron, positive ions, U.V. radiation X rays	Timing information
Scintillation detector	Emission of light	NaI	Gamma, high energy particles	Energy measurement
Solid organic scintillator	Emission of light	Anthracene, stilbene	Beta, protons	Detection of recoil photons
Liquid organic scintillator	Emission of light	Toluence	Beta, soft X rays	Detection of soft X-rays from element dissolved
Cherenkov counter	Emission of light	Glass, mica, cellophane	Electrons X-rays charged particles	Detection of X rays, to distinguish charged particles
Cloud chamber	Image forming device	Alcohol + water	Charged particles	Determination of energy
Bubble chamber	Image forming device	Propane, xenon, liquid H	Charged particles	Detection of very energetic particles, to study particle interaction
Spark chamber	Image forming device	Metallic plates	High energy charged particles	Localisation of trajectories
Photographic emulsion	Image forming device	Emulsion	Charged particles	Determination of energy and charge to study particle interaction

6.1. Parallel plate avalanche counter :

Parallel plate avalanche counters (PPAC) are transmission type gas counters known for their precise timing measurements. These cannot be used very efficiently to detect the light particles because of their low ionisation capabilities, however, the solid state detectors are best suited for them. Hence the avalanche counters are considered to be versatile detectors for heavily ionising particles [15], [16] whereas the solid-state detectors are not suitable for detecting the heavy charged particles due to the problem of radiation damage. Besides serving the purpose of time sensitivity, PPAC detectors have a resolution better than 200 psec. They have almost 100% detection efficiency and a good time resolution even at high counting rates. They can also be used in combination with large area position sensitive counters (multiwire chambers). These detectors do not undergo radiation damages and the total thickness of a counter can be kept rather low due to low operating gas pressures. The other advantage with these type of detectors is that they can be built in any geometry (circular, rectangular) and size (1 sq. inch to 1 sq. meter) depending on one's own requirements.

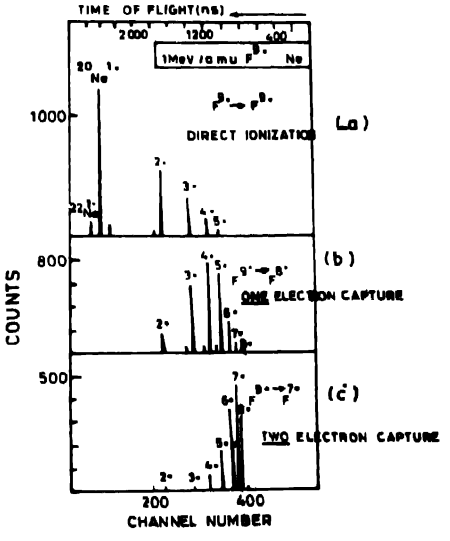

Figure 6. Spectra showing direct-ionisation, 1-electron capture and 2-electron capture in the collision of 1 MeV/amu F^{9+} + Ne collisions.

6.1.1. Principle of operation :

The counter consists of two plates (thin metallized foils) held parallel to each other shown in Figure 7. A high potential is applied across the two plates through which a gas is circulated at low pressures. The gap between the foils should be kept as small as possible to achieve a good time resolution. The ionising particle to be detected traverses the counter perpendicular to the foil-planes and produce ion-electron pairs in the counter gas. If 'E' is the potential applied across the plates and 'p' is the pressure of the gas contained between

the two plates, the ratio 'E/p' is so adjusted that a Townsend avalanche occurs uniformly anywhere in the counter volume on the passage of an ionising particle through it. The number of secondary electrons formed as a result of Townsend avalanche is given by

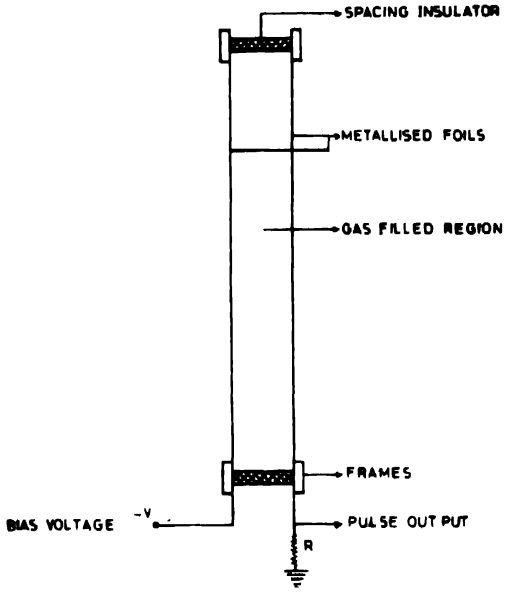

Figure 7. The principle of operation of the PPAC.

$$N = N_0 e^{\alpha d} \tag{13}$$

N_0 = Number of primary electrons formed.

d = Drift path length.

α = First Townsend coefficient.

The mean ionisation probability per unit path length,

$$= A \exp [-B(E/p)] \tag{14}$$

where A and B are constants for a specific gas. At low pressures, high value of α can be obtained from the reduced field strength (E/p=500 V/cm). This gives a gain upto 10^4. The few mV signal that is obtained from the parallel plate avalanche counter consists of

(i) a fast rising component due to motion of electrons.

(ii) and slow rising components stemming from positive ions with their much lower drift velocity.

The reason for this can be explained on the basis of the velocities of the electrons and that of positive ions. Once the ionisation starts, the electrons move towards the anode with drift velocity much higher than the velocity of positive ions which move towards the

cathode. Thus the electrons are collected quickly and induce a pulse with a fast rise time (rise time less than 2 nsec). The slow moving positively charged ions give a comparatively slow rising pulse (rise time approx. 1 microsec.) but having a higher amplitude. Only the fast rising pulse is utilised to register the instant at which the particle passes through counter and the slow rising pulse is differentiated out at the main amplifier.

The rise time of the pulse t_r is given by

$$t_r = x / v_e \tag{15}$$

where x = migration length,

v_e = velocity of electrons.

It is obvious from eq. (15) that for rise time of the pulse to be small, the migration length should be small and the drift velocity should be large. The electrons formed close to the foil thus contribute most to the pulse for which the migration length is the distance between the foils.

6.1.2. Optimum parameters :

(I) Gap between the two electrodes is usually kept between 1 mm and 3 mm. A gap less than 1 mm distorts the parallelism between the two foils due to the electrostatic forces. It is necessary for the two foils in the detector to be parallel otherwise the migration length will vary depending on the point where the particle deposits its energy to the counter and will consequently give different rise times. This would inturn deteriorate time resolution.

(II) The electrons drift velocity depends upon the E/p ratio. For electron drift velocity to be high. 'E' should be high and 'p' should be low. But 'E' greater than 3 KV is not suitable in order to avoid sparking problems as well as problems arising due to electrostatic forces. 'E' is chosen to be between 500 V to 3 KV.

Pressure 'p' less than 10 torr is undesirable because the number of primary ions formed is so small that no usable signal is obtained. However the maximum pressure is limited to 30 torr because a pressure greater than this would require the entrance and exit foils to be considerably thicker in order to avoid rupturing of the foils.

(III) The gas used in the detector should have a high coefficient of gas multiplication so that the number of electrons formed give rise to a usable signal. Best results have been obtained by using pure hydrocarbon gases, e.g. methylal, isobutane, isobutylene, pentane, heptane etc. The P–10 gas (90% Ar + 10% methane) is not used since it gives poor rise time. However the degree of purity of gas is not critical [15]. Use of isobutane's purity of 99.95% and 99.5% does not show any considerable difference in the performance. It is necessary to circulate the gas because during the passage of the ion through the gas some fragment products may be formed which can result in the deterioration of the detector's performance. Small variation in pressure however does not affect the performance considerably and the gas flow can be controlled using the needle valves. To increase the

number of primary electrons, the foil is coated with a material having a high secondary electron coefficient although this increases the effective thickness of the counter.

6.1.3. Typical description of a simple PPAC :

A simple parallel plate avalanche counter consists of two thin stretched metallized plastic foils mounted on supports and separated by spacers, the whole of which is immersed in a cell of circulating gas. This cell has a thin entrance and exit window. The metallised foils have to be rigorously parallel and even a low gas pressure of a few torr would make this requirement impossible. A voltage is applied between the two foils. Designs of PPAC's can be found in the literature [15–17].

6.1.4. Performance characteristics of PPAC :

(*i*) *Amplification :*

It is found that in all gases, high amplification is reached at low pressures. The electron drift velocity depends on eE/p. For low values of pressure (p), high values of E/p are reached implying high values of electron drift velocity which in turn increases the probability of inelastic collisions. The mean free path thus becomes shorter and amplification at large distances from the wire thus assumes higher values. It is found that the highest amplification is thus reached with isobutane because of its quenching properties and that the amplification factor varies very weakly; the, pulse height increases with the density of the gas. The signal amplitude varies linearly with the primary energy deposited in the counter and that the heavier is the particle the more is the energy deposited in the counter and greater the pulse height [15].

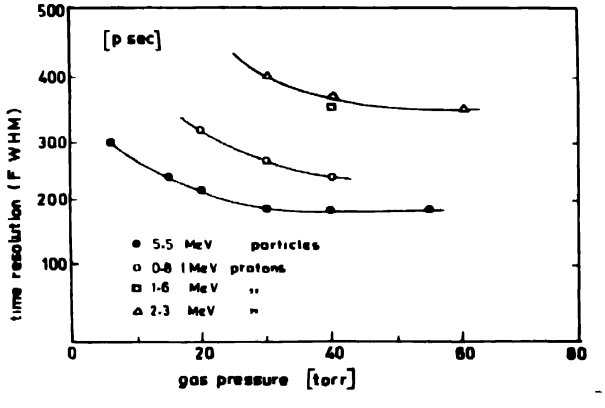

Figure 8. Dependence of the time-resolution of PPAC on gas pressure.

(*ii*) *Time resolution :*

The time resolution is measured by observing the delay between the pulses from the two counters by means of a Time to Amplitude Converter (TAC). A plot of time resolution versus gas pressure is shown in Figure 8.

It is shown that the operation of a PPAC at higher gas pressures results in excellent timing properties even for light particles. Table 5 gives an idea of the time resolution (in psec) of PPAC's with different geometries. The particles used in measurements are given in brackets.

From this table one can see that the time resolution of the PPAC becomes better as the gap between the foils is reduced for the same area. Also by increasing the area of the PPAC the time resolution is not affected and gets better for heavier particles.

Table 5. Time resolutions (p–sec) of parallel plate avalanche counters as a function of gap (mm) and area (cm^2).

Gap (mm)		Area (sq cm)	
		50	200
4		400 (alpha)	
		250 (16 0)	
2	320 (alpha)	320 (alpha)	350 (alpha)
1	280 (alpha)	280 (alpha)	
	160 (16 0)	160 (16 0)	

(*iii*) *Rise time :*

Rise time of the current pulses provides important information about the collection time of the electrons. For all gases tested the rise time increases with pressure. At low pressure the fastest rise time of a few nsec can be acheived.

6.2. Position sensitive PPAC :

In Time of Flight experiments using large area detectors a knowledge of polar and azimuthal scattering angles is required. This can be done in two ways :

(*i*) by combining a PPAC with a multiwire proportinal counter.

(*ii*) by making the PPAC position sensitive [18, 19].

6.2.1. Principle of operation :

The conductive cathode foil of a detector consists of horizontal strips. The position pulses induced on these strips are read out by the charge division method [18] and yield the position information of the particle along a direction (say Y-axis). In addition, a vertical set of parallel wires is placed between the anode and the cathode potentials. The positive signals sensed by these wires are read out by the charge division method and provide the X-position of the events. The timing signals derived from the wires are not disturbed by the various wires and strips.

A detailed description of the position sensitive PPAC's can be found in refs. [18] and [19]. However, some of the salient features of a position sensitive PPAC may be noted as follows;

(i) The position resolution of the detector remains unaffected even for counting rates as high as 10^5 counts per sec.

(ii) The time resolution of a position sensitive PPAC is nearly independent of the impinging point of the particles to be detected except for points very close to the detector's frame for which the time resolution gets worse.

(iii) There exists a linear relationship between internal delay time and displacement of the impact point of the particle from the end point of the detector. The propagation velocity of the timing signal turns out to be 2/3 of the velocity of light. Internal delay time is, however, affected by the mechanical imperfection in positioning the counter planes, or even the attractive electrostatic forces between the electrodes which tend to increase the gap between the large area detectors. Neither the wires nor the strips have noticeable effect on the internal time delay or on the intrinsic time resolution of the position sensitive counters.

In conclusion, we may mention that PPAC is an excellent timing detector having a time resolution of the order of psec and of 100% detection efficiency. These detectors can have any shape or size; are cheap, simple to build, insensitive to radiation damage and can handle events upto 10^5 counts per sec. They can also be used effectively to obtain position information. They have however the disadvantage of having large thickness of materials in the path of the beam thus causing large energy and angle straggling.

6.3. Micro-channel plate detector :

A Microchannel Plate (MCP) is an array of $10^4 - 10^7$ miniature electron multipliers oriented parallel to one another as shown in Figure 9. The channel diameters range form 10–100 micrometer and the length to diameter ratio of each channel is between 40–100. Channel axes are typically normal to or tilted at a small angle of eight degrees to the MCP

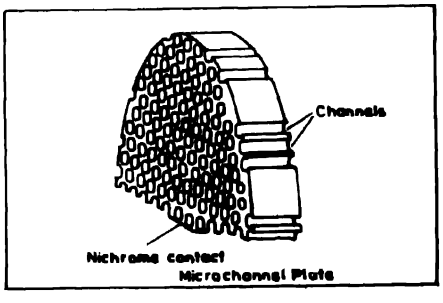

Figure 9. Cut view of a micro channel plate.

input surface. The material used for the fabrication of the channel matrix is lead treated so as to give maximum secondary electron characteristics of each channel and to render the channel walls semiconducting so as to allow charge replenishment from an external voltage source. The parallel electrical contact to each channel in the matrix is provided by depositing a metallic coating of Nichrome on the front and rear surfaces of the input and

output electrodes respectively. The total resistance between the two electrodes is approximately 10^9 ohms.

6.3.1. Construction :

As stated above, MCP comprises a matrix of single channel electron multipliers. The number of multipliers or channels and their dimensions are determined by resolution considerations. Generally, the channels are 8, 12 or 25 micrometer in diameter and the complete detector plate has a thickness of 1 mm and a diameter of 18–75 mm.

The material used for construction of the MCP is glass because it allows accurate control of channel diameter and regularity in the array. Also, the special glass used for constructing MCP has the conduction and secondary emission characteristics required for channel multiplication, as well as good stability and high vacuum performance. Generally a mixture of 50% lead oxide, 40% silicon dioxide and smaller quantities of several alkali oxides constitute the glass material. Glass of this composition has high electrical resistivity which can be removed by removing the oxygen from lead by reduction in an atmosphere of hydrogen gas for several hours at 400°C. Most of the reduced lead evaporates from the surface. The remaining lead coalesces into metallic cluster giving a characteristic black colour. The high secondary electron emission coefficient is caused by a layer consisting of silicion, oxygen, potassium and lead. The production of an MCP involves a multistep process; some important steps are listed in the following lines:

In the first stage a billet of channel glass and solid core is assembled. The purpose of the core is to prevent distortion and collapse of the channels during fusion stages and the diameter of the core rod is kept equal to the diameter of the internal glass tube. The core and channel glasses should have compatability w.r.t their expansion, viscosity, diffusion and solubility. The assembled billet is clamped to the feed mechanism and drawn slowly through the oven thus reducing the diameter from 35 mm to 0.8 mm. This fibre is then cut into lengths, stacked and fused into a symmetrical hexagonal shaped array. The bundle is then drawn a second time to produce hexagonal multifibre, again about 0.8 mm in diameter. This in turn is cut stacked in a hexagonal glass capsule and fused under vacuum. This fused stack is cut into slices and ground to the required shape and size and polished. The solid core glass is finally etched away leaving the channel matrix intact and ready for processing. The polished blanks are now baked in the reducing atmosphere to produce in each channel a resistive layer with the required secondary emission characteristics. Metallic layer of an alloy of Nickle and Copper is deposited onto polished surfaces of each plate which act as electrodes connecting all channels in parallel.

6.3.2. Theory of operation :

The theory of channel multiplication is covered by many authors. A computer model using Monte Carlo methods also predicts the performance of the straight channel multipliers.

However, a simple theory of operation of a straight channel electron multiplier is given below.

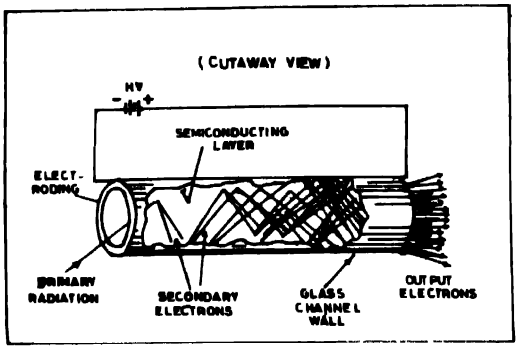

Figure 10. A straight channel electron multiplier.

Figure 10 gives the diagram of a straight channel multiplier. An incident electron produces δ secondary electrons. The parameters are such that δ^2 electrons are produced in the second stage, δ^3 electrons are produced in the third stage and so on Hence, the overall gain $G = \delta^n$ [20], assuming that the secondary emission is normal to channel walls gave the value of the gain as,

$$G = \left(\frac{AV}{2\alpha V_0^{1/2}} \right)^{4V_0\alpha^2/V} \tag{16}$$

V = Total channel voltage

V_0 = Initial energy of an emitted secondary electron ~ 1 eV.

α = Length to diameter ratio of the channel.

A = Proportionality constant in the assumed relation.

$S = AV_e^{1/2}$ where, V_e is the electron collision energy in eV and $A = 0.2$. As the applied voltage across the channel increases the secondary electron number also increases, since each collision then occurs at higher energy V_e. It is to be noted that the maximum gain obtained is of the order of 10^4 with a straight channel electron multiplier. Rather than exhibiting a maximum the curve levels off at large V_e due to secondary emission not orthogonal to the channel walls. The upper limit of the gain of a straight channel electron multiplier is set by the onset of the "ion feedback" which results in an unstable performance of the MCP. As the gain increases, the probability of producing positive ions at the output of the channel also increases. These ions are produced by the collision of the electrons with the residual gas molecules at ambient pressures greater than 10^{-6} torr and with gas molecules desorbed on the channel walls under electron bombardment. Such ions can drift back to the channel input producing ion after pulses.

The ion feedback can be reduced considerably by cascading two sets of channel arrays inclined at small angles. This configuration is called "Chevron".

The Chevron :

Ion feedback suppression in single channel multipliers can be achieved by curving the channel. The plates are oriented so that the channel bias angles (typically 0°/8° or 0°/15°) provide a sufficiently large change to inhibit the positive ions (see Figure 11). The gain thus increases from 10^4 in the case of straight channel electron multiplier to 10^7 in a chevron. The two plates in a Chevron are separated by 50-150 micrometer and individually operated at gains in 10^4 range. The effect of interplate bias voltage on output pulse height distribution and FWHM of the Chevron MCP has been investigated in detail [21]. He has found that a Chevron configuration exhibits high gains (greater than 10^7) because of the multiplicity of channels excited in MCP2, by a single channel in MCP1. Later studies performed on the curved channel MCPs with different values of separation and plate diameters have shown that the ion feedback effect for gains below 5×10^5 is not significant.

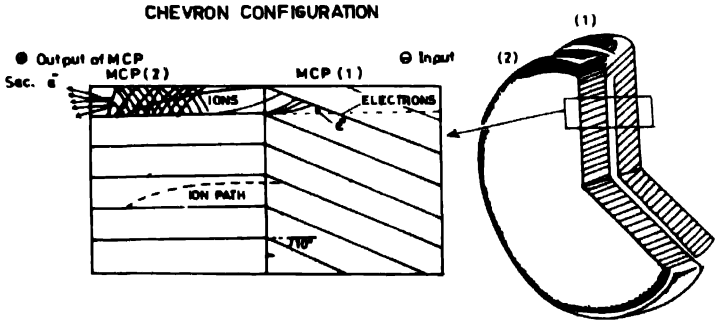

Figure 11. Micro-channel plates in Chevron configuration.

6.3.3. Performance characteristics :

Schagen [20] has summarized the detection efficiency of the channel multipliers for various kinds of primary radiation as given in Table 6.

Table 6. Detection efficiency and energy range of the MCP for different types of radiation

Type of radiation	Energy range	Detection efficiency
Electrons	0.2–2 keV	50–85%
	2–50 keV	10–60%
Positive ions	0.5–2 keV	5–85%
	2–50 keV	60–85%
U.V. radiation	300–1100 Å	5–15%
	1100–1500 Å	1–5%
Soft X-rays	2–50 Å	5–15%
Diagonistic X-Rays	0.12–0.2 Å	1%

Pulse height distribution :

The output pulse height distribution of an MCP is nearly an exponential function of the form

$$n(q) = n \exp(-\bar{q}/q) \tag{17}$$

where $n(q)$ = number of pulses with height q,

n = normalization factor,

$\bar{q}$ = mean gain of distribution. It is a function of voltage V over MCP.

The transfer characteristic is linear for output currents upto 10% of standing current (*i.e.* current flowing in the channel walls). For higher input currents, the plate begins to show saturation effects and the characteristic begins to level out. If the resistance of the plate remained constant, the output would saturate at a value close to the conduction current. The effective resistance of the plate however changes slightly in operation because the electron cascade forms a parallel resistive path. This produces a more gradual saturation effect and allows an output current to be drawn which can exceed the nominal conduction current of 1 microamp. As the individual multipliers of the plate are virtually independent of one another, each channel will saturate if the current drawn from it approaches its saturation current.

6.3.4. Transit time :

The transit time is defined as the time that elapses from the initial excitation to the attainment of a given current level at the output of a channel multiplier. It is a direct function of the channel length. Transit times are of the order of 1 nsec. The width of the pulse as in a Chevron configuration or the time spread as measured by 100 MHz oscilloscope amounts to a few nsec with a rise time of 0.5 nsec.

$$\text{Transit time} = 100\, l\ (\text{mm})/(VkV). \tag{18}$$

l = channel length

V = voltage applied across a MCP.

6.3.5. Noise :

If operated in carefully controlled conditions the background count rates can be acheived less than 1 count/sec.

6.3.6. Dark count :

Lead glass used in MCP has a high work function. Thus the output pulse rates from thermal emission is low. However at room temperatures the dark count from a Chevron configuration is about 1 count/sq cm/sec. Dark count begins to increase at pressures greater than 10 torr due to the ion feedback effects.

6.3.7. Lifetime :

The lifetime of an MCP is the lifetime during which the MCP behaves like a detector with a sufficient high detection efficiency and gain together with a low background count rate to ensure an efficient signal acquisition. Lifetime of an MCP can be influenced basically by two effects :

(*a*) *External causes :*

MCP should be exposed to atmosphere for a time as small as possible. They should be mounted and operated in a ultra high vacuum atmosphere. Particularly the input side where the conversion of primary electrons into secondary electrons takes place, can be damaged by both, mechanical as well as chemical effects. Hydrocarbons escaping from the diffusion pump oil may cause an irreversible loss of its gain.

(*b*) *Internal causes :*

The external causes mentioned above affect the conversion efficiency at the input side of MCP. The secondary emission coefficient of the surface of channel wall diminishes due to high density bombardment of clouds of secondary electrons. If a marked decrease in gain occurs, it is worthwhile to interchange the two plates. This degradation is related to total charge delivered per channel and is hardly dependent on charge density.

6.3.8. Dead time :

Each channel of an MCP has a dead time of about 10^{-2} sec. The fact that there are 10^5–10^6 channels in each plate which operate more or less independently of each other, the effective dead time of an MCP is 10^{-7}–10^{-8} sec provided no single channel is excited more frequently than once every 10^{-2} sec. *i.e.* the incident flux is distributed uniformly over the active area.

6.3.9. Magnetic Field Immunity :

Because of small dimensions and correspondingly high electric field strength, MCP should exhibit a high degree of immunity to the magnetic field.

6.4. Mounting of the MCP :

Various ways of mounting the MCP are available in the literature, see for example references [22–26]. The mounting arrangement [22] is shown in Figure 12. In this arrangement the foil and the plates are perpendicular to the ion beam, Electrons emitted from the foil are bent by 180° by applying a weak magnetic field or crossed electric and magnetic field to strike the MCP Prior to striking the plates the electrons are accelerated by an accelerator harp to 2 keV. The angular dispersion is reduced by using a collimator at 90° position of the bend. The suppression grid placed in front of the MCP reduces the tertiary electron emission when the secondary electrons are incident on a plate. The conical anode of

50 ohm characteristic impedence is used to reduce electrical reflections. Using this arrangement the authors were able to obtain time resolutions of 150 ps for 8.8 MeV helium ions and 90 psec for 104 MeV oxygen.

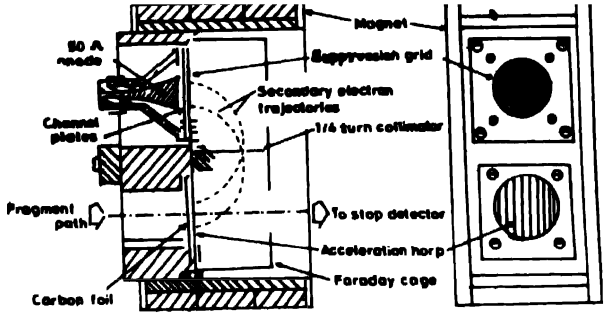

Figure 12. Micro-channel plates mounting [22].

The MCP can also be made position sensitive if the electron path is isochronous. This system was developed by Busch *et al* [26]. The position signal in this arrangement is obtained by charge division method.

6.5. Precautions in using the MCP :

(i) Long exposures to the ambient atmosphere and to the humidity should be avoided. They should be stored in clean atmosphere, preferably in a nitrogen flow box.

(ii) Polished surfaces should not be touched and the plates should not be placed on flat surfaces.

(iii) They should always be operated in a vacuum of the order of 10^{-5} torr or better. The pumping system should be oil free. If an oil diffusion pump is used a liquid nitrogen cold trap is preffered to prevent oil backstreaming.

(iv) While mounting, overlapping of the input and output contacts should be avoided.

(v) If low energy charged particles are to be detected, care should be taken to shield off from the electric fields produced due to the channel plates or its wiring.

In conclusion, it may be stated that the MCP's are excellent timing detectors yielding good time resolution (less than 100 ps) and are ideal as start detectors for TOF measurements. Further, they can be used for position information as well.

7. Summary

In this article, an overview of the production of heavy ions by the various particle accelerators is highlighted. An effort to bring out an exposition of the heavy ion 15 UD pelletron machine which has been recently installed as a "National Facility" at the Nuclear Science Centre (NSC), New Delhi, has been made. The relevent theoretical models to interpret the processes involved in multi-ionisation are also summarised. The PPAC and

MCP radiation detectors usually employed in accelerator based atomic physics experiments have been discussed with regard to their working principles, characterisation and energy time resolutions.

Acknowledgment

The authors acknowledge gratefully the encouraging support extended by the Department of Physics, Banaras Hindu University (BHU) in establishing the Atomic Physics Laboratory for conducting the atomic collision experiments in the department as well as at the Nuclear Science Centre (NSC), New Delhi. The authors wish to thank Prof G K Mehta, Prof A P Patro and the NSC scientific personnels for providing their valuable suggestions, comments and friendly cooperation. This work has been financially supported in part by a grant No. NSC/RKB/AUC/P–11, under University Grants Commission funding for the university projects at NSC, New Delhi and by the Department of Physics, BHU, Varanasi.

References

[1] R Shanker 1990 *Indian J. Pure Appl. Phys.* 28 51

[2] M Stanley Livingston 1969 *Particle Accelerators : A Brief History,* (Cambridge MASS : Harvard Press)

[3] G K Mehta and A P Patro 1988 *Nucl Instrum. Meth* A268 334

[4] H F Beyer and R Mann 1984 *Progress in Atomic Spectroscopy Part C* eds H J Beyer and H Kleinpoppen (New York : Plenum) p 397

[5] J H McGuire and L Weaver 1977 *Phys Rev* A16 41

[6] A Russek and M T Thomas 1958 *Phys Rev* 109 2015

[7] R E Olson, T J Gray, H G Berry, E B Halle and V D Irby 1987 *Phys. Rev. Lett* 59 36

[8] D Mathur, E Krishnakumar, F A Rajagara, U T Raheja and C Badrinathan 1990 *Intern. J Mass Spectros. Ion Processes* 99 237

[9] C L Cocke 1979 *Phys Rev.* A20 749

[10] T J Gray, C L Cocke and E Justiniano 1980 *Phys. Rev* A22 849

[11] A Muller, B Schuch, W Groh, E Salzborn, H F Beyer, P H Mokler and R E Olson 1986 *Phys. Rev.* A33 3010

[12] J C Levin, R T Short, C S O H Cederquist, S B Elston, J P Gibbons, I A Sellin and Schmidt Boecking – H 1987 *Phys Rev* A36 1649

[13] T Tonuma, H Kumagai, T Matsuo and H Tawara 1989 *Phys Rev.* A40 6238

[14] J Ullrich, Schmidt Boecking–H and C Kelbch 1988 *Nucl Instrum. Meth* A268 216

[15] H Stelzer 1976 *Nucl. Instrum. Meth.* 133 409

[16] A Breskin 1977 *Nucl. Instrum Meth.* 141 505

[17] A Breskin and N Zwang, 1977 *Nucl. Instrum. Meth* 144 609

[18] Y Eyal and H Stelzer 1978 *Nucl. Instrum. Meth.* 155 157

[19] L J Lyndgren and A Sandell 1983 *Nucl. Instrum Meth.* 219 149

[20] P Schagen 1974 *Advances in Image Pick Up and Display* Vol. 1 (New York : Academic) p 1

[21] J L Wiza 1979 *Nucl. Instrum. Meth.* 162 587

[22] A·M Zebelman, W G Meyer, K Halback, Poskanzer, R G Sextro, G Gabor and D A Landis 1977 *Nucl. Instrum. Meth.* 141 439

[23] T Nagakawa and W Bohne 1988 *Nucl Instrum. Meth.* 271 523

[24] J Girard and M Bolore 1977 *Nucl Instrum. Meth* 140 279

[25] F S Goulding and B G Harvay1975 *Ann. Rev. Nucl. Sci.* 25 203

[26] F Busch, W Pfeffer, B Kohlmeyer, D Schull and F Puhlhoffer 1980 *Nucl. Instrum. Meth.* 171 71

About the Reviewers

The author (R Shanker) is on faculty in the department of physics, faculty of science, Banaras Hindu University, Varanasi since 1985. He received his PhD degree in 1972 from B.H.U., and worked as a research associate at IIT Kanpur (1971-72) and at the University of New Brunswick and Dalhousie University, Canada (1973-77). He served as a Scientist-coworker at the University of Bielefeld, Germany from 1978 to 1984. Besides his earlier contributions in the works of high resolution spectroscopy of diatomic molecules, he has been active in the area of accelerator based atomic physics using keV to MeV particle accelerators for the last 15 years. His recent interest is directed to the studies of spectroscopy of highly charged slow-moving recoil ions in fast heavy-ion-atom collisions using the 15 UD Pelletron machine at the Nuclear Science Centre (NSC), New Delhi and to the atomic-field bremsstrahlung from keV energy electron colliding with free atoms and molecules at B.H.U., Varanasi.

The co-author M J Singh is a Senior Research Fellow (CSIR) who is presently conducting investigations on the recoil ions using a time-of-flight spectrometer at NSC, New Delhi.